JOURNAL OF THERMOPHYSICS AND HEAT TRANSFER
Vol. 23, No. 4, October–December 2009

Heat and Mass Transfer in Evaporator of Loop Heat Pipe

M. A. Chernysheva* and Y. F. Maydanik†
Institute of Thermal Physics, 620016, Yekaterinburg, Russia

DOI: 10.2514/1.43244

Investigation of heat-exchange processes in the evaporator of a loop heat pipe is important for the development of heat transfer devices with low thermal resistances. A two-dimensional mathematical model of the evaporator active zone is presented. Three modes of vapor generation in the wick have been examined, where each differs in the mechanism of the vapor phase formation and in the saturation of the capillary structure: 1) evaporation to the vapor grooves, 2) volumetric evaporation in the two-phase zone, and 3) volumetric evaporation in the two-phase zone separated from the heated wall of the evaporator by dried zones. Conditions identifying changes between modes have been formulated. Structural characteristics of the wick with different pore sizes have been taken into account. Using a numerical–analytical method, results were obtained for three copper loop heat pipes with biporous wicks, where the working fluid was water for one of the loop heat pipes and methanol for the other two. The heat-load dependent temperature drop between the evaporator wall and the vapor in the vapor grooves has been presented. Additionally, a comparative analysis of calculated and experimental results was performed.

Nomenclature

c_p	=	specific heat at constant pressure, $J/kg \cdot K$
h_{hv}	=	latent heat of vaporization, J/kg
K	=	permeability, m^2
k	=	thermal conductivity, $W/m \cdot K$
L	=	length, m
n	=	normal vector
P	=	pressure, Pa
Q	=	heat load, W
q_{in}	=	applied heat flux, $W \cdot m^{-2}$
R	=	thermal resistance, K/W
R, r	=	pore radius, m
T	=	temperature, °C
S	=	area, m
α	=	heat-exchange coefficient, $W/m^2 \cdot K$
ε	=	porosity
μ	=	dynamic viscosity, $Pa \cdot s$
ρ	=	density, kg/m^3

Subscripts

comp	=	compact
cond	=	condensation
cont	=	contact
dry	=	dry
ext	=	external
gr	=	vapor groove
l	=	liquid
ll	=	liquid line
nucl	=	nucleation
p	=	peak
q	=	active zone (heat input zone)
v	=	vapor
vl	=	vapor line
wall	=	evaporator wall (or case)
$1f$	=	single phase (saturated with liquid)
$2f$	=	two phase

Received 16 January 2009; revision received 19 May 2009; accepted for publication 20 May 2009.

*Ural Branch of the Russian Academy of Sciences, Amundsen Street, 106; mariya@itp.uran.ru.

†Professor, Ural Branch of the Russian Academy of Sciences, Amundsen Street, 106; maidanik@etel.ru.

I. Introduction

A LOOP heat pipe (LHP) is a two-phase heat transfer device using capillary pumping of the working fluid. It consists of an evaporator, a compensation chamber, vapor and liquid lines, and a condenser, as shown in Fig. 1, where the LHP principal design is presented. Detailed descriptions of the main working principles of LHPs are presented in [1–3]. The evaporator, the key element of an LHP, primarily determines the operation and performance of the device. The evaporator includes a wall, a wick, vapor grooves, and a liquid core passage. The evaporator is coupled to a compensation chamber, which receives liquid displaced from the condenser during LHP startup and operation. Heat is applied to the outer surface of the evaporator wall where it then is transferred though the wall and wick to the evaporating menisci. The generated vapor is collected in the vapor grooves and travels through the vapor line to the condenser. Liquid then returns to the compensation chamber through the liquid line. To reach the evaporating menisci, liquid flows back through the wick that separates the evaporation zone and the compensation chamber.

Investigations [4–7] have shown that the evaporating menisci creating the capillary pressure can be located both on the groove–wick surface and inside the wick. Mathematical models of heat and mass transfer processes in the evaporation zone consider this situation but at the same time most are based on the assumption of the structural uniformity of a wick, i.e., a wick having pores of the same size [8–14]. However, in actual LHP wicks there are pores of different sizes. In Fig. 2 a typical graph of pore-size distribution for a sintered titanium wick with a porosity of about 60% is presented as an example. Line A is the differential curve of pore-size distribution and B is the corresponding integral curve, where the differential function $\psi(r)$ can be obtained by $\psi(r) = d\Psi^*(r)/dr$. According to Fig. 2, the pore radius of this wick varies from 0.3 to 14 μm.

Figus et al. [15] developed a two-dimensional mathematical pore network model for a wick with a varying pore-size distribution. The pore network simulations indicated that in this case capillary effects could lead to fractal types of vapor-liquid fronts which cannot be predicted by a single pore-size model. A previous investigation [16] suggested a model of heat-exchange processes in an LHP evaporator, where structural characteristics of the wick were also taken into account. Based on the idea regarding different pore-formation modes in porous materials presented in [16] it was suggested using biporous wicks to allow a more advanced vapor removal system. The main

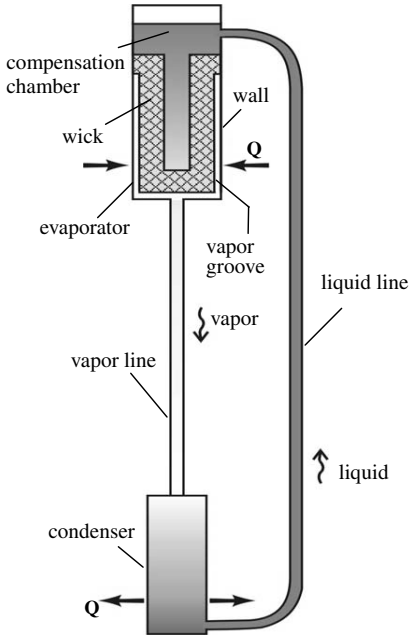

Fig. 1 Principal scheme of a loop heat pipe.

feature of a biporous wick is the pore-size distribution differential curve having two evident peaks, unlike monoporous wicks having characteristics shown in Fig. 2. An additional peak on the curve $f = F(r)$ means that in such a porous material pores of two primary sizes prevail. In this case, large pores serve as additional vapor removal paths in the evaporation zone, whereas small pores fill with the liquid and serve as the liquid conduit to the evaporating menisci. Vapor and liquid occupied pores in total form a two-phase zone with

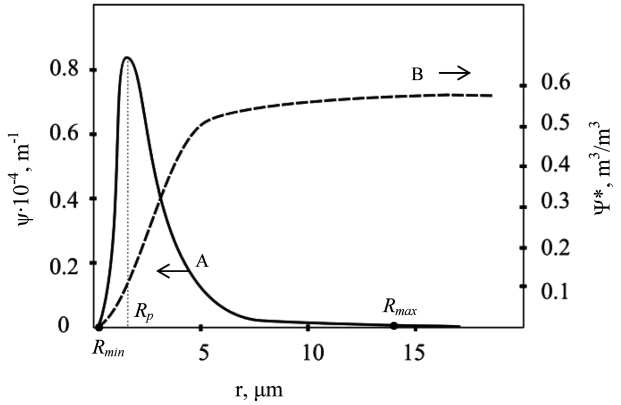

Fig. 2 Pore-size distribution; A: differential curve; B: integral curve.

an advanced evaporating surface that improves the heat-exchange conditions. The effectiveness of such an approach has been confirmed by both experimental and analytical investigations [17–20]. It was shown that biporous wicks in fact allow intensifying the heat-exchange processes in the evaporation zone of an LHP. The current investigation is a continuation of this research and topic. The model developed earlier has been adapted to the new configuration of the evaporation zone. Additionally, the calculation procedure used creates a new specified formulation of conditions for transformation of liquid occupied pores into vapor occupied pores.

II. Physical Model and Mathematical Formulation

In Fig. 3 a segment of the LHP evaporator is presented. Depending on the value of the applied heat load, three different operating conditions can exist in the evaporation zone. In the case of a low heat flux the evaporating menisci are at the wick–groove interface (Fig. 3a). The wick is completely saturated with liquid and the grooves are filled with vapor. At high heat flux, drying of large pores takes place and a two-phase layer forms, where both dry and saturated pores are found (Fig. 3b). When the heat load increases close to a critical value a dry layer in the wick can occur near the heated wall of the evaporator (Fig. 3c). The heat exchange in the evaporating zone becomes worse because the two-phase layer is separated from the heated wall by the vapor blanket. One of the main parameters characterizing the evaporation efficiency is the value of the evaporator thermal resistance, which is determined by the relation of the temperature difference between the temperature on the outer surface of the wall (T_{wall}) and the temperature of vapor in the groove (T_v) to the heat load:

$$R_{\text{ev}} = \frac{T_{\text{wall}} - T_v}{Q} \tag{1}$$

Correlations for the evaporator thermal resistance are given below in accordance with the three vaporization modes described earlier:

a) First mode:

$$R_{\text{ev}} = R_{\text{wall}} + R_{\text{cont}} + R_{1f} \tag{2}$$

b) Second mode:

$$R_{\text{ev}} = R_{\text{wall}} + R_{\text{const}} + R_{2f} \tag{3}$$

c) Third mode:

$$R_{\text{ev}} = R_{\text{wall}} + R_{\text{const}} + R_{\text{dry}} + R_{2f} \tag{4}$$

Examining the right side of Eqs. (2–4) for R_{ev} it is seen that two components always present do not depend on the evaporating mode, namely, the thermal resistance of evaporator wall R_{wall} and thermal contact resistance R_{cont}. The first is determined by the temperature difference between the internal and external evaporator walls. Increasing the thermal conductivity of the evaporator wall and decreasing the thickness decreases the value R_{wall}. The thermal

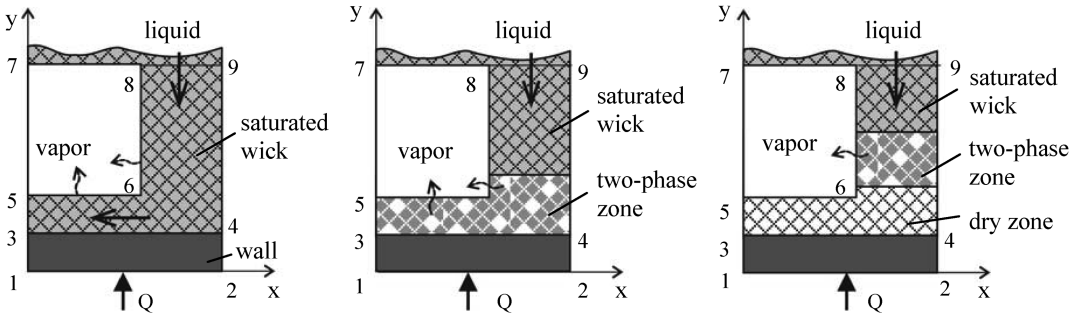

a) Evaporation in vapor groove **b) Vaporization into two-phase zone** **c) Vaporization into two-phase zone and partial wick drying**

Fig. 3 Scheme of vaporization modes.

contact resistance R_{cont} takes into account the imperfection of the thermal contact between the wick and the evaporator case. According to [16], specific quantities of R'_{cont} can vary from 3×10^{-5} to 7×10^{-5} m$^2 \cdot$ K/W. It should be noted that the values R_{wall} and R_{cont} depend only slightly on the location of the evaporating front. Thus, the contribution of these two components in the total evaporator thermal resistance R_{ev} can be considered constant values. Next, the other components of Eqs. (2–4) are examined. For the first evaporating mode, evaporating menisci serving as heat sinks are situated on the groove–wick interface and are separated from the hot evaporator wall by a layer of wetted wick. Thermal resistance of this layer is given as R_{1f} in Eq. (2) and determines the temperature difference between the external surface of the wick and the evaporating surface. For the second vaporization mode given by R_{2f} in Eq. (3), this is the thermal resistance of a two-phase evaporating layer where evaporating menisci are located. In accordance with the model of three-mode vaporization in the LHP evaporator, the second mode is the most effective compared to the two others. The enhanced heat exchange is first due to the increased quantity of the evaporating menisci involved in the heat-exchange process as the evaporating surface becomes more developed. Furthermore, in the second regime, evaporating menisci form a two-phase layer situated closer to the heated wall of the evaporator. Considering the third evaporation mode, the main characteristic taken into account is the presence of the dry wick zone near the evaporator wall and the displacement of the two-phase evaporating layer deep into the wick. As indicated previously, this negatively influences the effectiveness of the heat-exchange processes. Thus, the thermal resistance of the dry zone R_{dry} is included in the total thermal resistance for the third mode [see Eq. (4)]. The larger the dry zone, the greater the thermal resistance R_{dry}. In summary, it can be concluded that the intensity of heat-exchange processes substantially depends on the wick saturation condition and on the location of evaporating menisci.

The change between vaporization modes results from the drying of an amount of wick pores. One reason for the liquid to vapor pore transformation is boiling of the superheated liquid. In accordance with the nucleation theory described in [21], the formation of a vapor bubble with radius r_{nucl} is possible only if the liquid is superheated sufficiently relative to its equilibrium state. The lower bound of the nucleation superheat ΔT_{nucl} is determined by

$$\Delta T_{\text{nucl}} = \frac{2 \cdot \sigma \cdot T_s}{\rho_v \cdot r_{\text{nucl}} \cdot h_{\text{hv}}} \tag{5}$$

Another cause of pore dryout is an excessive hydrodynamic load on a meniscus, which can surpass its capillary potential. The capillary pressure ΔP_c is determined by

$$\Delta P_c = \frac{2 \cdot \sigma}{r_c} \tag{6}$$

and is used for pumping the working fluid during system operation. Thus, the second condition of dryout of a pore of radius r_c can be presented as follows:

$$\Delta P_{\text{LHP}} = \frac{2 \cdot \sigma}{r_c} \tag{7}$$

where ΔP_{LHP} is the total pressure drop in the LHP. The total pressure drop in the LHP includes the pressure difference in the wick, vapor grooves, vapor line, condenser, liquid line, and any gravitational head if the LHP is inclined:

$$\Delta P_{\text{LHP}} = \Delta P_{\text{wick}} + \Delta P_{\text{vg}} + \Delta P_{\text{vl}} + \Delta P_{\text{cond}} + \Delta P_{\text{ll}} + \Delta P_g \tag{8}$$

The wick pressure drop consists of two parts:

$$\Delta P_{\text{wick}} = \Delta P_{\text{out\_ev\_zone}} + \Delta P_{\text{ev\_zone}} \tag{9}$$

where $\Delta P_{\text{out\_ev\_zone}}$ is the pressure drop in the wick portion outside against the evaporation zone, i.e., above the boundary between points 7 and 9 (see Fig. 3) and $\Delta P_{\text{ev\_zone}}$ is the pressure drop in the evaporation zone, which depends on the evaporation mode, according to the proposed model. The transfer conditions from surface evaporation to vaporization in a two-phase layer are described by the inequalities:

$$\Delta T_{sh} \geq \Delta T_{\text{nucl}}(R_{\max}) \tag{10}$$

$$\Delta P_{\text{LHP}} \geq \Delta P_c(R_{\max}) \tag{11}$$

and conditions for the formation of a dry zone by the inequalities:

$$\Delta T_{sh} \geq \Delta T_{\text{nucl}}(R_{\min}) \tag{12}$$

$$\Delta P_{\text{LHP}} \geq \Delta P_c(R_{\min}) \tag{13}$$

where $R_{\max}$ and $R_{\min}$ correspond to the maximum and minimum pore sizes of the pore-size distribution curve.

The mathematical model is based on using several assumptions. First, the evaporation mode in the evaporation zone is assumed steady and stable. Additionally, local thermal equilibrium between the porous structure and the working fluid is assumed. Two separate systems of minichannels in the two-phase zone are modeled, where the first includes connected dry pores and the other consists of connected saturated pores. Vapor moves through the wick via dry pores and liquid flows via wet pores. Both the vapor and liquid flows are assumed to follow Darcy's law. The phase permeabilities for liquid and vapor flows in a two-phase layer are determined by the ratio between the quantity and the size of pores occupied with liquid or vapor, respectively. The prevailing motion of vapor and liquid is shown by arrows in Fig. 3. In the evaporation zone the liquid flows along the groove–wick surface. In a two-phase layer the vapor flow moves along the normal direction to the groove surface. Interfacial equilibrium is supported by surface tension. The computation model is two dimensional and the left and right borders of the computation domain are lines of symmetry. The convective component of heat transfer in the wick is assumed small compared to the conductive one. The effective thermal conductivity in a dry wick was calculated previously by Odelevski [22]:

$$k_{\text{wick}} = k_{\text{comp}} \cdot \frac{1 - \varepsilon}{(1 + \varepsilon)^b} \tag{14}$$

where k_{comp} is the thermal conductivity of the bulk material and the coefficient b in Eq. (14) was taken equal to 2.1. For a liquid saturated wick the effective thermal conductivity is given by

$$k_{\text{eff}} = k_{\text{wick}} + \varepsilon \cdot k_l \tag{15}$$

The effective thermal conductivity of a wick portion with a two-phase zone was determined using an average value between the effective thermal conductivity of a dry and a saturated wick:

$$k_{2f} = 0.5 \cdot (k_{\text{wick}} + k_{\text{eff}}) \tag{16}$$

Based on the above assumptions, the governing equations for vapor and liquid phases are presented next. The vapor and liquid flow in the single-phase regions of the wick, i.e., where the wick is saturated either with liquid or with vapor, are described by

$$u_l = -\frac{K}{\mu_l} \cdot \nabla P_{1f} \tag{17a}$$

and

$$u_v = -\frac{K}{\mu_v} \cdot \nabla P_{1f} \tag{17b}$$

where K is the permeability coefficient of the porous material. For sintered porous materials the permeability coefficient can be determined according to the following correlation:

$$K = C_k \cdot \varepsilon \cdot R_{\text{prob}}^2 \tag{18}$$

where C_k is a coefficient depending on the specific wick (for the wicks used in the current investigation C_k was specified as 0.5), R_{prob} is a breakdown radius of the wick. For cases of a two-phase zone, the governing relations, allowing for the different phase permeabilities for liquid and vapor, respectively, are given as

$$u_l = -\frac{K_l}{\mu_l} \cdot \nabla P_{2f} \tag{19a}$$

and

$$u_v = -\frac{K_v}{\mu_v} \cdot \nabla P_{2f} \tag{19b}$$

According to [22], phase permeability for liquid and vapor in a two-phase zone can be determined by

$$K_l = K \cdot \frac{\int_{R_{\min}}^{R^*} r^2 \cdot \psi(r)\mathrm{d}r}{\int_{R_{\min}}^{R_{\max}} r^2 \cdot \psi(r)\mathrm{d}r} \tag{20a}$$

and

$$K_v = K \cdot \frac{\int_{R^*}^{R_{\max}} r^2 \cdot \psi(r)\mathrm{d}r}{\int_{R_{\min}}^{R_{\max}} r^2 \cdot \psi(r)\mathrm{d}r} \tag{20b}$$

where R^* is a boundary meniscus radius, such that the boundary meniscus radius implies that pores with radii larger than R^* are filled with vapor. Correspondingly, pores with a radius less than R^* are filled with liquid. For the boundary radius R^* the value is taken to be equal to the minimum of r_{nucl} and r_c, which are, respectively, determined from Eqs. (5) and (7), or

$$R^* = \min(r_{\text{nucl}}, r_c) \tag{21}$$

The differential pore-size distribution for a monoporous wick is approximated by the relation:

$$\psi(r) = \frac{1}{2 \cdot \pi \cdot \chi} \cdot \exp\left(-\frac{(R_p - r)^2}{2 \cdot \chi}\right) \cdot C \tag{22}$$

where R_p is the pore radius at which the function $\psi = f(r)$ has a maximum or, in other words, the peak on the curve, and χ and C are approximation coefficients. For a biporous wick the approximation relation is given as a binomial:

$$\psi(r) = \frac{1}{2 \cdot \pi \cdot \chi_1} \cdot \exp\left(-\frac{(R1_p - r)^2}{2 \cdot \chi_1}\right) \cdot C_1 + \frac{1}{2 \cdot \pi \cdot \chi_1} \cdot \exp\left(-\frac{(R2_p - r)^2}{2 \cdot \chi_2}\right) \cdot C_2 \tag{23}$$

where $R1_p$ and $R2_p$ are the pore sizes corresponding to the first and second peaks, respectively, of the differential curve of pore distribution $\psi = F(r)$, and χ_1, χ_2, C_1, and C_2 are the corresponding approximation coefficients.

The energy equation for the evaporator wall is given by

$$\nabla^2 T_{\text{wall}} = 0 \tag{24}$$

The energy equation for a single-phase (wet or dry) wick is

$$\nabla^2 T_{\text{wick}} = 0 \tag{25}$$

And the energy equation for the two-phase regions is described by

$$k_{2f} \nabla^2 T_{\text{wick}} = -q'_{\text{ev}} \tag{26}$$

where q'_{ev} is the volumetric heat sink and it is assumed that the intensity of heat absorption is uniform at any point of a two-phase region.

The general boundary conditions for all regions are given next. For the boundary 1–2, the wall temperature gradient and heat the heat flux are related by

$$k_{\text{wall}} \cdot \frac{\partial T_{\text{wall}}}{\partial y} = -q_{\text{in}} \tag{27}$$

The heat flux q_{in} is calculated by taking into account the heat rate Q_{cp} required to increase the temperature of the liquid as it flows from the compensation chamber through the wick to boundary 8–9 of the evaporation zone:

$$q_{\text{in}} = \frac{Q - Q_{cp}}{S_q} \tag{28}$$

The velocity of the liquid flow at boundary 8–9 is taken as

$$u_{l,y} = \frac{Q - Q_{cp}}{2 \cdot \rho_l \cdot h_{\text{hv}} \cdot N_{\text{gr}} \cdot L_{\text{gr}} \cdot L_{89}} \tag{29}$$

where N_{gr} is the number of vapor grooves and L_{gr} is the groove length.

The temperature at boundary 7–9 equals the vapor temperature in a vapor groove:

$$T_{\text{wick}} = T_v \tag{30}$$

The vapor in the grooves is taken to be saturated, such that the vapor temperature can be defined as

$$T_v = T_{v\_\text{cond}} + \frac{\mathrm{d}T}{\mathrm{d}P} \Delta P_v \tag{31}$$

where T_{v_cond} is the vapor saturation temperature in the condenser. The vapor pressure drop ΔP_v includes the pressure drop in the vapor grooves, in the vapor line, and in the vapor section of the condenser:

$$\Delta P_v = \Delta P_{\text{vg}} + \Delta P_{\text{vl}} + \Delta P_{v\_\text{cond}} \tag{32}$$

Boundaries 1–7 and 2–9 are lines of symmetry so that

$$\frac{\partial T_{\text{wall}}}{\partial x} = 0 \tag{33}$$

and

$$\frac{\partial T_{\text{wick}}}{\partial x} = 0 \tag{34}$$

In the wick area along these symmetry boundaries the velocities are

$$u_{l,x} = 0, \qquad u_{v,x} = 0 \tag{35}$$

The boundary conditions for the wick depend on the specific phase conditions existing in the wick. In the case of the first evaporation mode, boundary 5–6 is given as

$$k_{\text{eff}} \cdot \frac{\partial T_{\text{wick}}}{\partial y} = q_{\text{ev}} \tag{36}$$

$$u_{v,y} = \frac{q_{\text{ev}}}{h_{\text{hv}} \cdot \rho_v} \tag{37}$$

and for boundary 6–8:

$$k_{\text{eff}} \cdot \frac{\partial T_{\text{wick}}}{\partial x} = q_{\text{ev}} \tag{38}$$

$$u_{v,x} = \frac{q_{\text{ev}}}{h_{\text{hv}} \cdot \rho_v} \tag{39}$$

In the case of the second mode the fact that the intensity of heat exchange during volumetric evaporation is much higher than under heat transfer at the groove–wick surface is taken into account. For this reason the following conditions for the boundaries 5–6 and 6–8 are used:

$$\frac{\partial T_{\text{wick}}}{\partial y} = 0 \tag{40}$$

and

$$\frac{\partial T_{\text{wick}}}{\partial x} = 0 \tag{41}$$

The same conditions (40) and (41) are used for a dry zone and a two-phase zone of the wick for the third evaporation mode.

The boundary 3–4 is represented by

$$k_{\text{wall}} \cdot \frac{\partial T_{\text{wall}}}{\partial y} = k \cdot \frac{\partial T_{\text{wick}}}{\partial y} \tag{42}$$

where k equals k_{eff} for a saturated wick, $k = k_{\text{wick}}$ for a dry wick, and $k = k_{2f}$ for a two-phase wick.

At the boundary between two regions in the wick the general condition is

$$k \cdot \frac{\partial T_{\text{wick}}}{\partial n} = k_{2f} \cdot \frac{\partial T_{\text{wick}}}{\partial n} \tag{43}$$

where k means k_{eff} for a saturated wick or k_{wick} for a dry wick.

The presented model was solved using a numerical–analytical method. In the first stage of the computational procedure for every value of heat load Q, the vapor temperature in vapor removal grooves T_v was calculated by Eq. (31). Then, the temperature field in the evaporation zone was calculated. To this effect a computational grid was created that covered a typical domain of the evaporation zone. A control volume method was used for discretization of the governing equations of the heat-mass transfer process in the computation domain. A vaporization mode in every control volume around the node was chosen using criteria (7–10). During this procedure the calculated boundary pore radius in the control volume R^* was compared with the values of maximum $R_{\max}$ and minimum $R_{\min}$ of the pore-size distribution curve $f = F(r)$.

The computation output was the temperature field in the evaporation zone. The intensity of the heat-exchange processes was estimated using the temperature difference ΔT between the wall temperature T_{wall} and the vapor temperature in the grooves T_v. The average temperature of the exterior evaporator case was used as T_{wall}. In conformity with the typical domain considered here, the value T_{wall} was determined as the mean along boundary 1–2.

III. Results and Discussion

Numerical results were obtained for three copper loop heat pipes, with one using water and the other two using methanol as the working fluid. The LHPs also differed in terms of the wick pore sizes, where all wicks were made from sintered copper powder. Differential curves of the pore-size distributions for each wick are shown in Fig. 4. According to the graph, the wick of LHP2 can be characterized as the most macroporous of all wicks presented here, whereas the most microporous wick is that of LHP3. At the same time all curves exhibit a bimodal form. Hence, all wicks can be characterized as biporous and all have almost the same porosity of about 70%. Exact porosity values are shown in Table 1.

All other main design parameters of the LHPs were identical. The geometrical parameters of evaporators, vapor lines, condensers, and liquid lines are highlighted in Table 2.

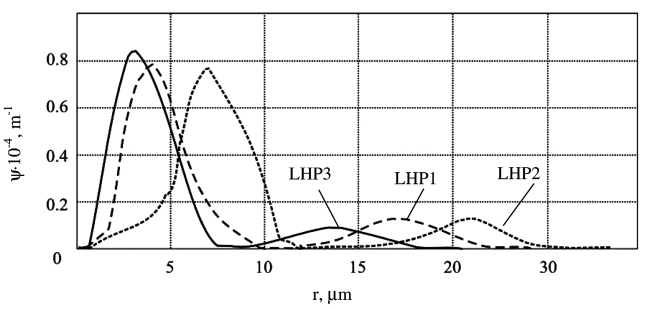

Fig. 4 Differential curves of the wick pore-size distribution for LHP1, LHP2, and LHP3.

Table 1 Distinctive features of LHPs and wicks

	LHP1	LHP2	LHP3
Porosity ε, %	69	70	68
Wick	Midporous	Macroporous	Microporous
Working liquid	Water	Methanol	Methanol

Table 2 Main geometrical parameters of LHPs

Length of vapor line, mm	350
Length of liquid line, mm	900
Outer diameter/inner diameter of vapor line, mm	5/4
Outer diameter/inner diameter of liquid line, mm	5/4
Heating zone area, cm^2	16
Length of active zone, mm	40
Evaporator wall thickness, mm	0.5
Wick thickness, mm	6
No. of vapor grooves	12
Length of vapor grooves, mm	40
Cross section of vapor grooves, mm × mm	1.8 × 1.8
Evaporator wall/wick material	Cu/Cu
Heat sink and ambient temperature, °C	20
LHP orientation	Horizontal

The geometrical parameters of a typical domain were as follows: $L_{1-2} = 1.7$ mm, $L_{1-3} = 0.5$ mm, $L_{3-5} = 0.4$ mm, $L_{5-6} = 0.9$ mm, and $L_{5-7} = 1.8$ mm. The model results for the investigated LHPs are presented in Fig. 5 for heat-load dependence of the temperature difference ΔT. To evaluate the accuracy of the model experimental data are also presented in Fig. 5. The good correlation between the analytical results and the experiment data provides validation that the proposed model effectively describes the vaporization processes in the evaporation zone of an LHP.

It should be noted that the behavior of the curves $\Delta T = f(Q)$ presented in Fig. 5 is different for water and methanol LHPs, where the curve for the water LHP in the range of heat loads is linear. This monotone growth of the temperature difference in the evaporation zone as the heat load increases points to a lack of any critical change in the character of the heat and mass transfer processes. However, the results for LHPs with methanol (nos. 2 and 3) have a different character. Overall, the behavior of the two methanol LHPs is similar, so it can be characterized as consistent behavior. Namely, each of these curves has an inflection point that conditionally divides the results into two distinct parts with different inclination angles. At the same time, at low heat loads, the behavior of the methanol LHPs is situated quite close to each other and to that of LHP1 with water, where the temperature differences are almost the same. When the heat load exceeds 30 W the behavior of the methanol LHPs changes, such that the increase in temperature difference is much sharper for increasing heat loads. Such a change in the behavioral dynamics of LHPs 2 and 3 indicates the existence of processes in the evaporation zone that affect adversely the heat transfer conditions.

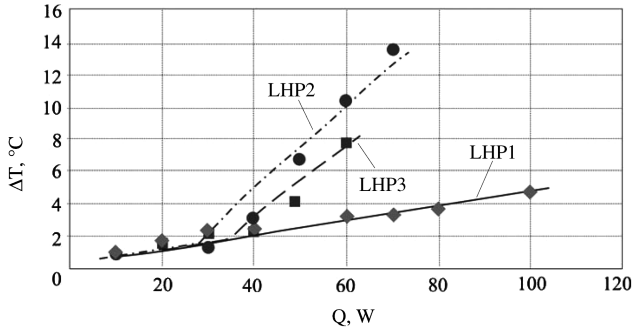

Fig. 5 Temperature difference ΔT as a function of the heat load. Experimental data: diamonds, circles, and squares; calculated data: solid, dashed, and dot-dashed lines.

According to the model the reason for such behavioral changes of the relation $\Delta T = f(Q)$ for methanol LHPs is an appearance of local dry zones close to the evaporator wall. As the wicks have different structural characteristics, the dynamics of the pore dryout processes differ as well. Transformation of liquid-filled pores to vapor-filled pores occurs with a slight delay in LHP2 compared with LHP3. This results from the presence of smaller pores in the wick of LHP3, which can withstand higher liquid superheats and higher pressure gradients. As a result, under equivalent heat loads the temperature difference in the evaporation zone of LHP2 is higher compared with LHP3, which is supported by the results presented in Fig. 5. Thus, the structural characteristics of the porous material directly influence the heat-exchange processes in the evaporation zone of an LHP.

In contrast to methanol, a transition from the second vaporization mode to the third was not observed for water in the tested range of heat loads. The dryout of the wick layer situated near the heated wall is not observed as water has better thermophysical properties compared with methanol. A significant role in this case is played by surface tension, which is 3 times greater for water than for methanol. The level of superheat in the range of heat load Q turns out to be insignificant for the appearance of dry regions in the evaporator of the water LHP. This is supported by data presented in Fig. 6, where the values of nucleation superheat ΔT_{nucl} calculated by Eq. (5) are presented for varying pore sizes at a temperature T_s of 80°C. Hence, the influence of the working fluid properties on the vaporization mechanism and on the dynamics of the evaporation mode can be shown to be very significant. Thus, it is necessary to take this factor into account when selecting the LHP working fluid.

One additional factor that influences the heat-exchange processes in the LHP evaporator needs to be considered, which is the configuration of the evaporation zone. In this investigation, this was modified compared with the previous investigation [17]. A distinctive feature of the new configuration is that between the vapor grooves and the evaporator wall there is a wick layer, as shown in Fig. 3. In the previous case no wick layer was present under the region 5–6 and the vapor grooves were directly adjacent to the heated evaporator wall. Thus, it was decided to make configuration modifications of the evaporating zone. The function of the additional wick layer is to facilitate enhanced vaporization in the evaporation zone due to the increased evaporation surface area. In this case, a positive effect can be expected only when two conditions are fulfilled. First, this layer should be saturated with liquid to provide an evaporation zone. Given that, the evaporating menisci can be located both on the surface of this wick layer and within the wick layer. Secondly, the layer thickness should be minimized to minimize the impact on thermal resistance.

It was found that such a configuration of the evaporation zone is efficient only for the case of water. According to the calculations, over the entire range of examined heat loads, LHP1 did not experience a full dryout of the wick layer under the vapor groove. Whereas with methanol, this layer functioned only under low heat loads followed by it becoming dry with increasing heat loads. Such a transformation of the evaporation zone adversely affected the heat transfer processes. An exclusion of a reasonably large area from the active evaporation process resulted in increasing heat load on the wick segment located between two neighboring grooves. The evaporating menisci forming the two-phase evaporating layer were then located only in this area. After the dryout of the wick layer situated under the groove, the configuration of the evaporation zone becomes similar to the zone considered in [17]. It should be mentioned that such a transformation of the evaporation zone was not detrimental to the operation of LHPs 2 and 3 as operational capability was not lost. But, as can be seen from Fig. 5 for methanol, starting from a heat load of 30 W the heat transfer effectiveness in the evaporation zone decreases, which resulted in an abrupt increase of the wall to vapor temperature difference. This resulted in the thermal resistance of the evaporator and of the entire LHP to increase. In this case it becomes clear that even a partial dryout of the layer near the wall is quite critical for the heat exchange in the evaporation zone and, thus, is extremely undesirable during LHP operation.

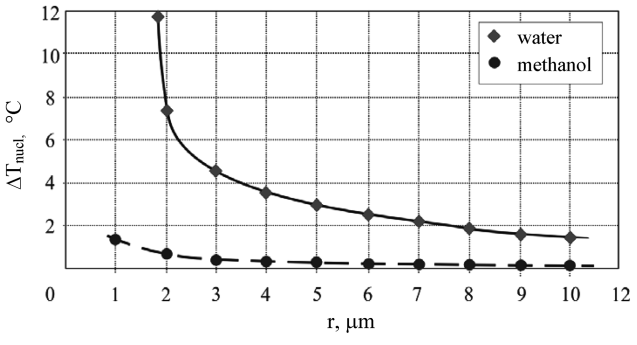

Fig. 6 Nucleation superheat as a function of pore size.

IV. Conclusions

The heat and mass transfer processes in the evaporator of a loop heat pipe were examined. A two-dimensional mathematical model of the evaporation zone of an LHP evaporator was developed. Solutions of the heat and mass transfer were obtained for three modes of vapor generation: evaporation at the wick–groove interface, evaporation in a two-phase zone, and evaporation in a two-phase region coupled to a vapor zone. The wick structural characteristics, including porosity and pore-size distribution of the porous material, were taken into account.

The model was used for investigation of copper LHPs using both methanol and water as the working fluids. The direct effects of working fluid properties on the evaporation mechanism were examined. The results of the model and experiment data compared very favorably and showed that the behavior and intensity of heat transfer depend on the structural characteristics of the capillary porous materials. Satisfactory agreement between the model results and experimental data confirms that the model provides a good description of the evaporation processes in the LHP evaporation regions.

Acknowledgment

This work was supported by the Russian Foundation for Basic Research, Grant No. 05-08-01180.

References

[1] Maydanik, Y. F., "Loop Heat Pipes," *Applied Thermal Engineering*, Vol. 25, Nos. 5-6, 2005, pp. 635–657. doi:10.1016/j.applthermaleng.2004.07.010

[2] Maidanik, Y. F., and Fershtater, Y. G., "Theoretical Basis and Classification of Loop Heat Pipes and Capillary Pumped Loops," Preprint of the *Tenth International Heat Pipe Conference*, Stuttgart, Germany, 1997, Keynote Lecture X-7.

[3] Ku, J., "Operating Characteristics of Loop Heat Pipes," Society of Automotive Engineers Paper 1999-01-2007, 1999.

[4] Demidov, A. S., and Yatsenko, E. S., "Investigation of Heat and Mass Transfer in the Evaporation Zone of a Heat Pipe Operating by the 'Inverted Meniscus' Principle," *International Journal of Heat and Mass Transfer*, Vol. 37, No. 14, 1994, pp. 2155–2163. doi:10.1016/0017-9310(94)90317-4

[5] Liao, Q., and Zhao, T. S., "A Visual Study of Phase-Change Heat Transfer in a Two-Dimensional Porous Structure with a Partial Heating Boundary," *International Journal of Heat and Mass Transfer*, Vol. 43, No. 7, 2000, pp. 1089–1102. doi:10.1016/S0017-9310(99)00212-4

[6] Zhao, T. S., and Liao, Q., "On Capillary-Driven Flow and Phase-Change Heat Transfer in a Porous Structure Heated by a Finned Surface: Measurements and Modeling," *International Journal of Heat and Mass Transfer*, Vol. 43, No. 7, 2000, pp. 1141–1155. doi:10.1016/S0017-9310(99)00206-9

[7] Dupont, V., Van Oost, S., Barremaecker, L., and Legros, J. C., "EBoWIT—EHP Characterization Device for Capillary Evaporator Development," *Proceedings of the Fourteenth International Heat Pipe Conference*, Federal University of Santa Catarina, Florianopolis, Brazil, 2007, pp. 95–100.

[8] Altman, E. I., Mukminova, M. I., and Smirnov, H. F., "The Loop Heat Pipe Evaporators Theoretical Analysis," *Proceedings of the Twelfth International Heat Pipe Conference*, Institute of Thermal Physics, Yekaterinburg, Russia, 2002, pp. 159–164.

[9] Qian, J., and Xuan, Y., "Numerical Investigation on Evaporator for Capillary Pumped Loops," *Proceedings of the Seventh International Heat Pipe Symposium*, Korean Society of Mechanical Engineers, Jeju, Korea, 2003.

[10] Figus, C., Le Bray, Y., Bories, S., and Prat, M., "Heat and Mass Transfer with Phase Change in a Porous Structure Partially Heated: Continuum Model and Pore Network Simulations," *International Journal of Heat and Mass Transfer*, Vol. 42, No. 14, 1999, pp. 2557–2569. doi:10.1016/S0017-9310(98)00342-1

[11] Takahashi, A. R., Oliveira, A. A., and Bazzo, E., "Analysis of Heat and Mass Transfer with Phase Change," *Proceedings of the Seventh International Heat Pipe Symposium*, Korean Society of Mechanical Engineers, Jeju, Korea, 2003.

[12] Ren, C., Wu, Q., and Hu, M., "Heat Transfer with Flow and Evaporation in Loop Heat Pipe's Wick at Low or Moderate Heat Fluxes," *International Journal of Heat and Mass Transfer*, Vol. 50, Nos. 11–12, 2007, pp. 2296–2308. doi:10.1016/j.ijheatmasstransfer.2006.10.029

[13] Kaya, T., and Goldak, J., "Numerical Analysis of Heat and Mass Transfer in the Capillary Structure of a Loop Heat Pipe," *International Journal of Heat and Mass Transfer*, Vol. 49, Nos. 17–18, 2006, pp. 3211–3220. doi:10.1016/j.ijheatmasstransfer.2006.01.028

[14] Coquard, T., Prat, M., de Tournemine, A. L., and Figus, C., "Pore-Network Models as a Tool for the Analysis of Heat and Mass Transfer with Phase Change in the Capillary Structure of Loop Heat Pipe," *Proceedings of the Fourteenth International Heat Pipe Conference*, Federal University of Santa Catarina, Florianopolis, Brazil, 2007, pp. 353–358.

[15] Figus, C., Ounougha, L., Bonzom, P., Supper, W., and Puillet, C., "Capillary Fluid Loop Developments in Astrium," *Proceedings of the Twelfth International Heat Pipe Conference*, Institute of Thermal Physics, Yekaterinburg, Russia, 2002, pp. 120–125.

[16] Vershinin, S. V., Fershtater, Y. G., and Maidanik, Y. F., "Effect of Contact Thermal Resistance on Heat Exchange During Evaporation from Small-Pored Capillary Structures," *Teplofizika Vysokikh Temperatur*, Vol. 30, No. 4, 1992, pp. 811–817 (in Russian).

[17] Chernysheva, M. A., Maydanik, Y. F., and Vershinin, S. V., "Heat Exchange in the Evaporator of a Loop Heat Pipe with a Biporous Capillary Structure," *Proceedings of the Eleventh International Heat Pipe Conference*, Japan Association for Heat Pipes, Tokyo, Japan, 1999, pp. 348–354.

[18] Semenic, T., and Catton, I., "Boiling and Capillary Limit Enhancement of a Heat Pipe Wick Using Biporouse Capillary Structure," *Proceedings of the Thirteenth International Heat Transfer Conference*, Sydney Convention and Exhibition Centre, Sydney, Australia, 2006, Paper PRT-18.

[19] Yeh, C., Chen, C., Lui, B., and Chen, Y., "Effect of the Pore Size Distribution of the Biporous Wick in Loop Heat Pipe," *Proceedings of the Ninth International Heat Pipe Symposium*, Monash University, Selangor, Malaysia, 2008, pp. 196–203.

[20] North, M. T., Sarraf, D. B., Rosenfeld, J. H., Maidanik, Y. F., and Vershinin, S. V., "High Heat Flux Loop Heat Pipes," *Proceedings of the Sixth European Symposium on Space Environmental Control Systems*, European Space Agency, Noordwijk, The Netherlands, 1997, pp. 371–376.

[21] Skripov, V. P., *Metastable Liquids*, Halsted Press, New York, 1974.

[22] Kovalev, S. A., and Solovev, S. L., *Evaporation and Condensation in Heat Pipes*, Nauka, Moscow, Russia, 1989, pp. 47–54.